Two-Dimensional Antiferroelectricity in Nanostripe-Ordered In_2Se_3

Chao Xu,[1] Yancong Chen,[2] Xiangbin Cai,[3] Arno Meingast,[4] Xuyun Guo,[1] Fakun Wang,[5] Ziyuan Lin,[1] Tsz Wing Lo,[1] Christian Maunders,[4] Sorin Lazar,[4] Ning Wang,[3] Dangyuan Lei,[6] Yang Chai,[1] Tianyou Zhai,[5] Xin Luo,[2,*] and Ye Zhu[1,†]

[1]*Department of Applied Physics, The Hong Kong Polytechnic University, Hung Hom, Hong Kong, China*
[2]*State Key Laboratory of Optoelectronic Materials and Technologies, Centre for Physical Mechanics and Biophysics, School of Physics, Sun Yat-sen University, Guangzhou 510275, China*
[3]*Department of Physics and Center for Quantum Materials, The Hong Kong University of Science and Technology, Clear Water Bay, Hong Kong, China*
[4]*Thermo Fisher Scientific, Achtseweg Noord 5, 5651 GG Eindhoven, The Netherlands*
[5]*State Key Laboratory of Material Processing and Die & Mould Technology, School of Materials Science and Engineering, Huazhong University of Science and Technology, Wuhan 430074, China*
[6]*Department of Materials Science and Engineering, City University of Hong Kong, 83 Tat Chee Avenue, Hong Kong, China*

(Received 28 November 2019; revised 14 March 2020; accepted 17 June 2020; published 22 July 2020)

Two-dimensional (2D) layered materials have been an exciting frontier for exploring emerging physics at reduced dimensionality, with a variety of exotic properties demonstrated at 2D limit. Here, we report the first experimental discovery of in-plane antiferroelectricity in a 2D material $\beta'-In_2Se_3$, using optical and electron microscopy consolidated by first-principles calculations. Different from conventional 3D antiferroelectricity, antiferroelectricity in $\beta'-In_2Se_3$ is confined within the 2D layer and generates the unusual nanostripe ordering: the individual nanostripes exhibit local ferroelectric polarization, whereas the neighboring nanostripes are antipolar with zero net polarization. Such a unique superstructure is underpinned by the intriguing competition between 2D ferroelectric and antiferroelectric ordering in $\beta'-In_2Se_3$, which can be preserved down to single-layer thickness as predicted by calculation. Besides demonstrating 2D antiferroelectricity, our finding further resolves the true nature of the $\beta'-In_2Se_3$ superstructure that has been under debate for over four decades.

DOI: 10.1103/PhysRevLett.125.047601

van der Waals (vdW) layered materials, with natural confinement in two dimension (2D), offer unprecedented opportunities to preserve or even enhance functionalities from 3D bulk down to single-layer thickness [1,2]. These functionalities can be further integrated in heterostructure devices made of a stack of distinct 2D materials [3,4]. There has been exciting progress in discovering 2D structures or phases with various functionalities, including ferromagnetism [5], superconductivity [6], and ferroelectricity [7,8], offering a wealth of choices for making 2D heterostructure devices. One recent example has been the demonstration of 2D ferroelectric materials including $CuInP_2S_6$ and WTe_2 [8–12], promising for making ultrathin flexible ferroelectric devices [13]. As the counterpart of ferroelectricity, antiferroelectricity has also been predicted in 2D materials such as $CuInP_2S_6$, competing with ferroelectric phases for the ground state [14,15]. The nature of 2D antiferroelectric ordering and the competition or transition between 2D ferroelectric and antiferroelectric phases are of significant interest for both fundamental understanding and phase-transition device applications [16,17]. However, despite several theoretical studies, potential antiferroelectric ordering in 2D materials has not yet been explored experimentally [14,15,18].

In this work, we demonstrate experimentally antiferroelectricity in a 2D material In_2Se_3. As the two stable phases at room temperature, $\alpha-In_2Se_3$ and $\beta'-In_2Se_3$ both have 2D structure consisting of [Se-In-Se-In-Se] quintuple layers bonded by vdW force [19,20]. Just recently, $\alpha-In_2Se_3$ has attracted great attention for its room-temperature 2D ferroelectricity down to single-layer thickness [11,21–24]. 2D ferroelectricity has also been reported in $\beta'-In_2Se_3$ [25,26], but still under debate [27] largely owing to its structural ambiguity: compared to $\alpha-In_2Se_3$, $\beta'-In_2Se_3$ is distinguished by its characteristic superstructure consisting of periodic nanostripes, the detailed atomic structure of which remains unclear [28,29]. Underpinning this structural ambiguity is the difficulty in solving large superstructures containing too many atoms by conventional diffraction analysis. Here, we adopt real-space imaging and electric polarization mapping based on scanning transmission electron microscopy (STEM), consolidated by first-principles calculations, to interrogate the structural ambiguity in $\beta'-In_2Se_3$. This allows us to disclose the nature of its superstructure to be 2D antiferroelectric ordering, rather than previously proposed ferroelectricity [25,26]. A ferroelectric-antiferroelectric competition is also revealed, which

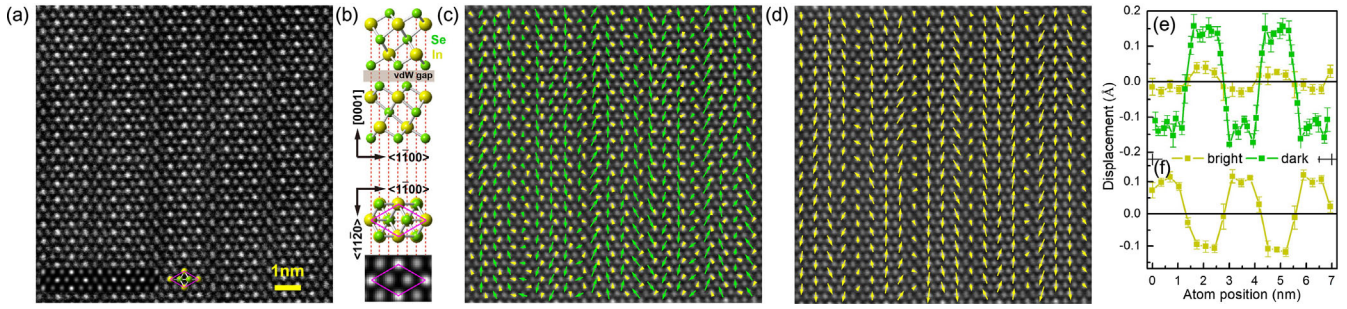

FIG. 1. (a) Plan-view ADF-STEM image of a $\beta'-In_2Se_3$ flake. The bottom-left inset is a multislice-simulated image. (b) Models of the basic $\beta'-In_2Se_3$ structure. (c) Atomic displacement map derived from (a) with respect to the reference lattice. The yellow (green) arrows are for bright (dark) columns. Displacement of only half of the dark columns is shown, with the other half being similar (see Fig. S4 in SM [30]). (d) Relative displacement map of bright columns with respect to the centers of the surrounding six dark columns. (e) Displacement profiles of bright and dark columns vertically averaged from (c). (f) Relative displacement profile of bright columns vertically averaged from (d). Error bars indicate ± 1 s.d.

can be preserved down to single-layer $\beta'-In_2Se_3$ as predicted by calculation.

Figure 1(a) is an annular dark-field (ADF) STEM image showing the [0001]-projected structure of $\beta'-In_2Se_3$. Atomic columns with different intensity are visible, with the brighter columns containing more In atoms that are heavier than Se. Both plan-view and cross-sectional [Fig. S1 in Supplemental Material (SM) [30]] STEM images are largely consistent with a high-temperature In_2Se_3 phase—2H $\beta-In_2Se_3$ with hexagonal symmetry [29,32]. However, different from the high-temperature β phase, room-temperature $\beta'-In_2Se_3$ exhibits additional periodic nanostripes along $\langle 11\bar{2}0\rangle$, each $\sim$1.4 nm wide (or $4d_{1\bar{1}00}$) and separated by dark boundaries containing elongated atomic columns [Fig. 1(a)]. Such nanostriped superstructure spans the whole $\beta'-In_2Se_3$ grain and its long-range ordering gives rise to satellite diffraction at $n/8$ $1\bar{1}00$ positions [Figs. S2(a) and S2(b) in SM [30]]. The structure of $\beta'-In_2Se_3$ can thus be interpreted as the parent $\beta-In_2Se_3$ structure plus the nanostriped superstructure. Note that the nearly identical basic structure of β- and $\beta'-In_2Se_3$ is also reflected by their similar Raman signals and electronic properties [20,40], and has led to contradictory phase identification in literature [20,26,28,40]. We follow the convention defined by van Landuyt *et al.* who first discovered the nanostriped superstructure and named it as $\beta'-In_2Se_3$ [28]. Throughout this manuscript, both "unit-cell" and crystallographic indexing refer to the parent structure, instead of the complicated superstructure.

The origin of $\beta'-In_2Se_3$ superstructure, the in-plane antiferroelectric ordering, is unveiled by atomic displacement mapping shown in Fig. 1. The sub-Angstrom resolution of aberration-corrected STEM allows a direct determination of atomic-column positions in Fig. 1(a) and the further derivation of atomic displacement with picometer precision [41–44]. Comparing with the reference lattice without superstructure (Fig. S3 in SM [30]), we can see collective atomic displacement primarily along $\langle 11\bar{2}0\rangle$, as illustrated in Fig. 1(c). It forms a transverse displacive modulation wave with a wavelength of two nanostripe width ($8d_{1\bar{1}00}$), consistent with the observed satellite diffraction. More strikingly, the dark atomic columns show much larger displacement than the bright columns [Fig. 1(e)]. As the dark columns are negatively charged (In:Se = 1:2) while the bright columns are positively charged (In:Se = 2:2), the larger cooperative displacement of dark columns should lead to charge-center separation and spontaneous electric polarization, just like conventional ferroelectrics $BaTiO_3$ and $BiFeO_3$ [45,46]. The polarization field can be reflected by mapping the relative displacement of bright columns with respect to the centers of the surrounding 6 dark columns [42,44], as shown in Figs. 1(d,f): the well-aligned displacement within individual nanostripes manifests ferroelectric ordering, whereas the periodic antiparallel displacement between neighboring nanostripes forms an unexpected antiferroelectric ordering, resolving the atomistic origin of the $\beta'-In_2Se_3$ superstructure that has been a mystery since 1975 [20,25,28].

We note that although many nanostripes are $4d_{1\bar{1}00}$ wide, $5d_{1\bar{1}00}$-wide nanostripes are also present which can alter the superstructure period and generate satellite diffraction different from $n/8$ $1\bar{1}00$, such as $n/9$ $1\bar{1}00$ and even incommensurate $n/8.5$ $1\bar{1}00$ as shown in Fig. S2 in SM [30]. Nevertheless, such a structure variation does not change the overall antiferroelectric ordering, as evidenced in Figs. S4(d) and S5(b) in SM [30]. The superstructure period does not depend on sample thickness (Fig. S6 in SM [30]), which distinguishes it from "superdomain" structure that usually exhibits larger and thickness-dependent domain widths [47]. No atomic displacement is detected along the out-of-plane direction in cross-sectional STEM images (Fig. S1 in SM [30]), thus the antiferroelectric polarization in $\beta'-In_2Se_3$ is predominantly in plane, along $\langle 11\bar{2}0\rangle$. Note that this polarization direction is 90° away from the previously proposed ferroelectric polarization [25].

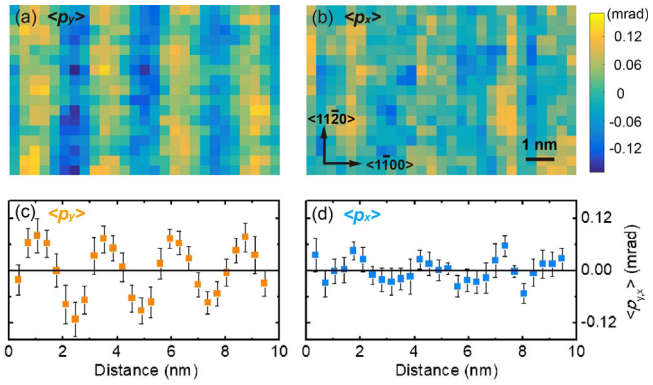

FIG. 2. Polarization mapping using EMPAD-based 4D STEM. Centers of mass (a) $\langle p_y \rangle$ and (b) $\langle p_x \rangle$ measured from CBED patterns. (c), (d) Vertically averaged $\langle p_y \rangle$ profile from (a) and $\langle p_x \rangle$ profile from (b). Error bars indicate ± 1 s.d.

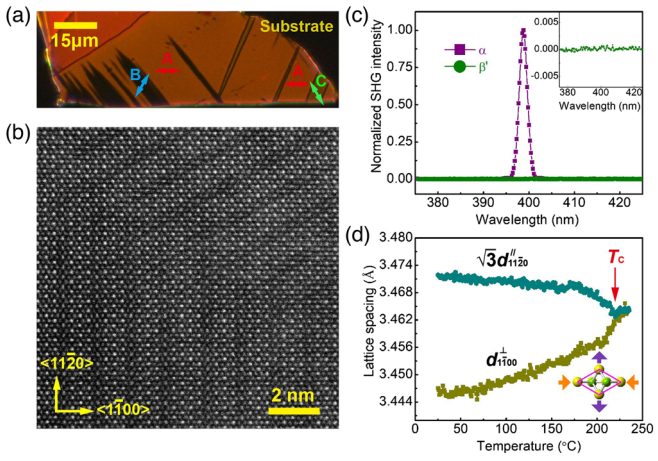

FIG. 3. (a) Polarized-light image of a $\beta'-In_2Se_3$ flake, with the polarization directions labeled. (b) ADF STEM image of 120° twin domains in $\beta'-In_2Se_3$, showing the switching of nanostripe direction across a coherent domain boundary. (c) SHG intensity of $\beta'-In_2Se_3$ showing no detectable response, in contrast to the strong SHG signal from ferroelectric $\alpha-In_2Se_3$. (d) Thermal variation of lattice spacings measured from electron diffraction during *in situ* heating.

To further verify the observed antiferroelectric ordering, we map directly the polarization field using 4D STEM performed on the newly developed electron microscopy pixel array detector (EMPAD) [38]. The symmetry breaking due to polarization leads to asymmetric intensity in a convergent-beam electron diffraction (CBED) pattern [37], which can be sensitively measured by EMPAD-based 4D STEM to map the polarization field (see Methods and Fig. S7 in SM [30]). The polarization map in Fig. 2(a) shows eminently the nanostripe pattern with antiparallel polarization along nanostripes and negligible perpendicular polarization, consistent with the displacement map in Fig. 1(d). Note that an electron probe larger than the basic unit cell was used for 4D STEM to avoid disk overlapping in CBED patterns for more accurate measurements [38]. The gradual polarization change across nanostripes in Fig. 2(c), in contrast to the relatively sharp change in the displacement profile in Fig. 1(f), can be attributed to the larger probe size and the reduced mapping resolution.

With all the nanoscale evidence presented above, we next try to demonstrate antiferroelectricity in $\beta'-In_2Se_3$ on a larger scale. However, owing to the large current leakage possibly from the small band gap (~0.8 eV) or Se vacancies, it is difficult to do conventional $P-E$ loop measurement on $\beta'-In_2Se_3$ [20,40]. Instead, we performed optical measurement to interrogate its antipolar structure. The linear-polarized-light images in Fig. 3(a) reveal three types of domains in $\beta'-In_2Se_3$, all showing linear-dichroism behavior as depicted in Fig. S9 in SM [30]. The domain contrast arises from different polarization directions, with an angular difference of 60°/120° between each other as labeled in Fig. 3(a). Such a domain structure has been interpreted as ferroelectric domains previously [25]. However, our STEM observation evinces that it actually reflects the structural anisotropy raised by antiferroelectric nanostripe ordering: with the three equivalent $\langle 11\bar{2}0 \rangle$ directions in the hexagonal parent structure ([11$\bar{2}$0], [1$\bar{2}$10], and [$\bar{2}$110]), nanostripes may orient along one of them in each domain and form three types of domains seen in Fig. 3(a). This atomistic origin of the domain structure is unveiled explicitly by atomic-resolution STEM imaging shown in Fig. 3(b). Such domain structure is antiferroelectric rather than ferroelectric, as further evidenced by second harmonic generation (SHG) measurement in Fig. 3(c): $\alpha-In_2Se_3$ gives strong SHG signal confirming its ferroelectricity [23], whereas no detectable SHG signal comes from $\beta'-In_2Se_3$, proving unambiguously its zero net polarization from antiferroelectricity, instead of the previously proposed ferroelectricity [25].

Besides the identified antiparallel displacement and polarization, as well as the domain structure, lattice distortion in $\beta'-In_2Se_3$ is also detected by a comparison with the parent $\beta-In_2Se_3$ phase using *in situ* heating in TEM. The in-plane hexagonal symmetry of $\beta-In_2Se_3$ requires $d_{1\bar{1}00} = \sqrt{3}d_{11\bar{2}0}$ that is indeed observed by electron diffraction at above 220 °C [Fig. 3(d)]. In contrast, for the room-temperature $\beta'-In_2Se_3$ phase, the lattice spacing for (1$\bar{1}$00) perpendicular to nanostripes, denoted as $d^{\perp}_{1\bar{1}00}$, is considerably smaller than $\sqrt{3}d^{\parallel}_{11\bar{2}0}$ along nanostripes, demonstrating symmetry breaking owing to lattice distortion. Upon heating, both an increase of $d^{\perp}_{1\bar{1}00}$ and a decrease of $d^{\parallel}_{11\bar{2}0}$ are observed in Fig. 3(d), until 220 °C when $\beta'-In_2Se_3$ transforms into $\beta-In_2Se_3$ with $d^{\perp}_{1\bar{1}00} = \sqrt{3}d^{\parallel}_{11\bar{2}0}$. Therefore compared to the parent $\beta-In_2Se_3$, lattice distortion in $\beta'-In_2Se_3$ involves two components: elongation along nanostripes (larger $d^{\parallel}_{11\bar{2}0}$) and compression perpendicular to nanostripes (smaller $d^{\perp}_{1\bar{1}00}$). Such lattice distortion resembles closely the classical

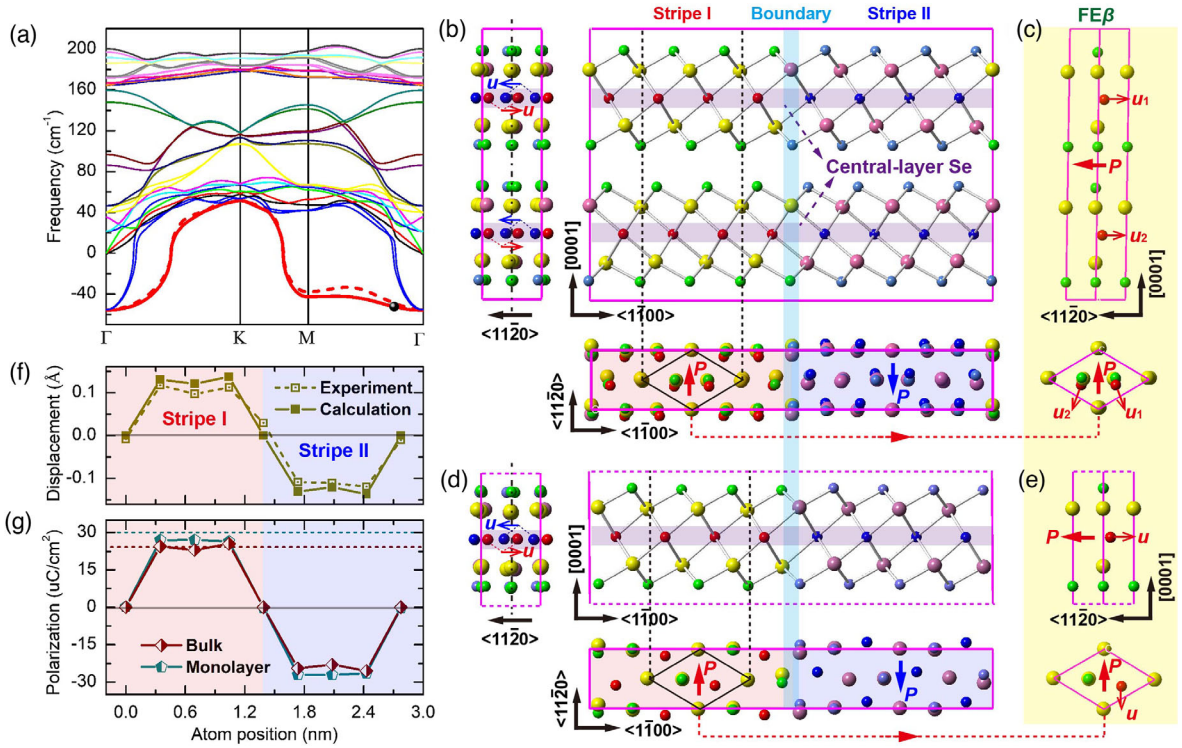

FIG. 4. (a) Phonon dispersion of parent bulk 2H $\beta-In_2Se_3$ showing structural instabilities associated with the soft modes of the lowest branch (red solid line) along the $\Gamma-M$ direction. The black dot indicates the soft mode generating the antiferroelectric β' phase. (b) Calculated antiferroelectric β' and (c) ferroelectric FEβ structure for bulk In_2Se_3. (d) Calculated antiferroelectric β' and (e) ferroelectric FEβ structure for single-quintuple-layer In_2Se_3. The FEβ structure is remarkably similar to the local structure within the $\beta'-In_2Se_3$ nanostripes, as indicated by the black unit-cell frames. (f) Relative displacement profile of bright columns measured from the simulated ADF STEM image based on the calculated structure in (b), compared to the experimental profile. (g) Polarization profiles across nanostripes of bulk and single-quintuple-layer $\beta'-In_2Se_3$, calculated from the structure in (b) and (d). The dashed lines indicate the calculated polarization of bulk and single-quintuple-layer FEβ phase for comparison.

tetragonal distortion in $BaTiO_3$ and $PbTiO_3$ and the rhombohedral distortion in $BiFeO_3$, which lower the unit-cell symmetry and couple with polarization along the elongation directions [45,46]. In $\beta'-In_2Se_3$, the detected antiferroelectric polarization is also along the elongation distortion. In fact, the lattice distortion and the antiferroelectric superstructure and domains disappear concomitantly, all at above 220 °C as revealed by *in situ* heating [Figs. 3(d), S10 and S11 in SM [30]], further confirming the coupling between them.

We also performed first-principles calculations to better understand the experimental observation on $\beta'-In_2Se_3$. Starting with the parent $\beta-In_2Se_3$, its phonon dispersion [Fig. 4(a)] reveals numerous structural instabilities, implying potential phase transitions at lower temperature [12,18,48]. The soft modes of the lowest branch (red solid curve) forms a "flat" region along the $\Gamma-M$ direction, which may "freeze" at lower temperature and generate superstructure with modulated atomic displacement [16]. The typical $\beta'-In_2Se_3$ superstructure has the wave vector $1/8\{1\bar{1}00\}$, which is indeed within the flat region as marked by the black dot in Fig. 4(a). Modulating the parent $\beta-In_2Se_3$ with this mode successfully leads to the antiferroelectric $\beta'-In_2Se_3$ [Fig. 4(b)] with excellent agreement with experimental observation. Based on the calculated $\beta'-In_2Se_3$ structure, a simulated ADF STEM image is overlaid in Fig. 1(a), which reproduces all the structural characteristics: (i) As shown in Fig. 4(f), the calculated atomic-column displacement quantitatively matches the experimental measurement in both magnitudes and the sharp changes at nanostripe boundaries. (ii) The central-layer Se atoms in each quintuple layer show much larger displacement than other atoms (also see Fig. S12 in SM [30]). Since the central-layer Se atoms belong to dark columns containing less In, this fully explains the measured larger displacement of dark columns. The dominant displacement of the central-layer Se atoms, together with their large Born effective charge ($-3.87\,e$), generates spontaneous antiparallel polarization $\sim$23–26 $\mu C/cm^2$ along $\langle 11\bar{2}0\rangle$ and the observed antiferroelectricity. (iii) The calculated atomic displacement is mostly in phase between the two quintuple layers, except at nanostripe boundaries where the opposite displacement is identified [Figs. S12(d) and S12(e) in SM [30]]. Such antiparallel atomic displacement is presumably a low-energy boundary configuration

to accommodate the polar discontinuity from antipolar nanostripes. This also results in elongated columns in [0001]-projected images, with considerably lower intensity owing to the disruption of electron probe channeling along the unaligned columns [49,50]. (iv) The flatness of the lowest branch along the $\Gamma-M$ direction suggests that superstructure with similar atomic displacement but different periodicity may form, fully consistent with the coexistence of $4d_{1\bar{1}00}$- and $5d_{1\bar{1}00}$-wide nanostripes imaged in Figs. S2–S5 in SM [30].

Then why does $\beta'-In_2Se_3$ exhibit such nanostriped antiferroelectric ordering? Antiferroelectricity is usually believed to arise from competition between structural and ferroelectric instabilities, with the latter being modulated by the former [16,51]. The ferroelectric instability is indeed identified by calculation based on the lowest-frequency mode at Γ point, which predicts a new ferroelectric In_2Se_3 phase with uniform polarization $\sim 24\ \mu C/cm^2$ along $\langle 11\bar{2}0\rangle$ [referred to as FE$\beta-In_2Se_3$ as shown in Fig. 5(c)]. Note that FE$\beta-In_2Se_3$ has a different structure from $\alpha-In_2Se_3$ and has never been experimentally observed. Actually, its structure is almost identical to the local structure within a nanostripe in $\beta'-In_2Se_3$, as illustrated in Figs. 4(b) and 4(c). Both phases manifest polarization dominated by $\langle 11\bar{2}0\rangle$ displacement of the central-layer Se atoms, with nearly the same displacement and polarization magnitudes [Fig. 4(g)], indicating the same type of polar instability shared by them. As for the structural instability, it is represented by the "flat" region along the $\Gamma-M$ direction that tends to modulate the Γ-point ferroelectric instability and generate antiferroelectricity. The flat region shares similar frequencies to the Γ point, suggesting that the driving forces to form ferroelectric and antiferroelectric ordering are comparable. The competition is then reflected by modulation periods, or the nanostripe widths, with the longer periods being more ferroelectric (toward Γ point with complete ferroelectric ordering) and the shorter periods being more modulated and antiferroelectric. The observed $4d_{1\bar{1}00}$ to $5d_{1\bar{1}00}$ width of nanostripes should represent the balance of the competition. With such compromised antiferroelectricity, $\beta'-In_2Se_3$ has the energy 2.5 meV/formula-unit lower than FE$\beta-In_2Se_3$, which explains the observed $\beta'-In_2Se_3$ as the stable phase. We note that even though a similar mechanism was proposed in conventional 3D antiferroelectrics [16,51], the competition between ferroelectric and antiferroelectric ordering, both are confined in 2D, has never been demonstrated unequivocally before.

Finally, with the remarkable agreement between experiments and calculations, we use the calculation to explore whether antiferroelectricity in $\beta'-In_2Se_3$ can be preserved down to single-layer thickness. Excitingly, even single-quintuple-layer $\beta'-In_2Se_3$ exhibits the same antiferroelectric ordering [Fig. 5(d)], originating from the soft mode in the flat phonon branch [Fig. S13(b) in SM [30]]. Its $\langle 11\bar{2}0\rangle$ polarization is even enhanced ($\sim$26–27 $\mu C/cm^2$) compared to bulk $\beta'-In_2Se_3$ [Fig. 5(g)]. The stability of 2D antiferroelectric ordering at this limit thickness is further verified by the 2.3 meV/formula-unit lower energy of single-quintuple-layer $\beta'-In_2Se_3$ compared with the corresponding FE$\beta-In_2Se_3$.

In summary, we have demonstrated experimentally in-plane antiferroelectricity in $\beta'-In_2Se_3$, in quantitative agreement with first-principles calculations. The identified antiferroelectricity is unique: It is in-plane dominated and confined in the single $\beta'-In_2Se_3$ quintuple layer, as opposed to conventional 3D antiferroelectrics such as $PbZrO_3$, and other 2D materials whose antiferroelectric ordering arises from antipolar stacking along the out-of-plane direction. Such 2D confinement enables the preservation of antiferroelectricity down to single-quintuple-layer thickness. Furthermore, the revealed competition between 2D ferroelectric and antiferroelectric ordering, as reflected by the nanostripe width, is unprecedented and suggests bright prospects for realizing antiferroelectric-ferroelectric phase switching in $\beta'-In_2Se_3$. At last, $\beta'-In_2Se_3$ is also known as a semiconductor with the band gap $\sim$0.8 eV and was demonstrated to make phase-switching memory devices [52]. The accurate structure model achieved in our work is essential for better understanding its emerging functionalities as a low-band-gap 2D antiferroelectric material.

Y. Z., N. W., D. Y. L., and Y. C. are thankful for the financial support from the Research Grants Council of Hong Kong (No. 15305718, No. C6021-14E, No. 16306818, No. 15303718 and No. 15201617). X. L. is thankful for support from NSFC (No. 11804286 and No. 11832019), the Fundamental Research Funds for the Central Universities (No. 19lgpy263), and the resources of the National Supercomputer Center in Guangzhou. T. Y. Z. is thankful for support from NSFC (No. 21825103). Y. Z is thankful for the helpful discussion from Dr. Zhen Chen and Dr. Yi Zhang. Technical support of the high-resolution electron microscopy facility at MCPF of HKUST is hereby acknowledged.

*luox77@mail.sysu.edu.cn
†yezhu@polyu.edu.hk

[1] V. Nicolosi, M. Chhowalla, M. G. Kanatzidis, M. S. Strano, and J. N. Coleman, Science **340**, 1226419 (2013).
[2] M. Chhowalla, H. S. Shin, G. Eda, L.-J. Li, K. P. Loh, and H. Zhang, Nat. Chem. **5**, 263 (2013).
[3] A. K. Geim and I. V. Grigorieva, Nature (London) **499**, 419 (2013).
[4] K. S. Novoselov, A. Mishchenko, A. Carvalho, and A. H. C. Neto, Science **353**, aac9439 (2016).
[5] C. Gong, L. Li, Z. Li, H. Ji, A. Stern, Y. Xia, T. Cao, W. Bao, C. Wang, Y. Wang, Z. Q. Qiu, R. J. Cava, S. G. Louie, J. Xia, and X. Zhang, Nature (London) **546**, 265 (2017).
[6] J. M. Lu, O. Zheliuk, I. Leermakers, N. F. Q. Yuan, U. Zeitler, K. T. Law, and J. T. Ye, Science **350**, 1353 (2015).

[7] K. Chang, J. Liu, H. Lin, N. Wang, K. Zhao, A. Zhang, F. Jin, Y. Zhong, X. Hu, W. Duan, Q. Zhang, L. Fu, Q.-K. Xue, X. Chen, and S.-H. Ji, Science **353**, 274 (2016).

[8] F. Liu, L. You, K. L. Seyler, X. Li, P. Yu, J. Lin, X. Wang, J. Zhou, H. Wang, H. He, S. T. Pantelides, W. Zhou, P. Sharma, X. Xu, P. M. Ajayan, J. Wang, and Z. Liu, Nat. Commun. **7**, 12357 (2016).

[9] Z. Fei, W. Zhao, T. A. Palomaki, B. Sun, M. K. Miller, Z. Zhao, J. Yan, X. Xu, and D. H. Cobden, Nature (London) **560**, 336 (2018).

[10] A. Belianinov, Q. He, A. Dziaugys, P. Maksymovych, E. Eliseev, A. Borisevich, A. Morozovska, J. Banys, Y. Vysochanskii, and S. V. Kalinin, Nano Lett. **15**, 3808 (2015).

[11] Y. Zhou, D. Wu, Y. Zhu, Y. Cho, Q. He, X. Yang, K. Herrera, Z. Chu, Y. Han, M. C. Downer, H. Peng, and K. Lai, Nano Lett. **17**, 5508 (2017).

[12] S. Yuan, X. Luo, H. L. Chan, C. Xiao, Y. Dai, M. Xie, and J. Hao, Nat. Commun. **10**, 1775 (2019).

[13] X. Wang, P. Yu, Z. Lei, C. Zhu, X. Cao, F. Liu, L. You, Q. Zeng, Y. Deng, C. Zhu, J. Zhou, Q. Fu, J. Wang, Y. Huang, and Z. Liu, Nat. Commun. **10**, 3037 (2019).

[14] J. R. Reimers, S. A. Tawfik, and M. J. Ford, Chem. Sci. **9**, 7620 (2018).

[15] M. A. Gave, D. Bilc, S. D. Mahanti, J. D. Breshears, and M. G. Kanatzidis, Inorg. Chem. **44**, 5293 (2005).

[16] A. K. Tagantsev, K. Vaideeswaran, S. B. Vakhrushev, A. V. Filimonov, R. G. Burkovsky, A. Shaganov, D. Andronikova, A. I. Rudskoy, A. Q. R. Baron, H. Uchiyama, D. Chernyshov, A. Bosak, Z. Ujma, K. Roleder, A. Majchrowski, J. H. Ko, and N. Setter, Nat. Commun. **4**, 2229 (2013).

[17] B. Xu, J. Íñiguez, and L. Bellaiche, Nat. Commun. **8**, 15682 (2017).

[18] C. Xiao, F. Wang, S. A. Yang, Y. Lu, Y. Feng, and S. Zhang, Adv. Funct. Mater. **28**, 1707383 (2018).

[19] S. Popovic, A. Tonejc, B. Grzeta-Plenkovic, B. Celustka, and R. Trojko, J. Appl. Crystallogr. **12**, 416 (1979).

[20] X. Tao and Y. Gu, Nano Lett. **13**, 3501 (2013).

[21] W. J. Ding, J. B. Zhu, Z. Wang, Y. F. Gao, D. Xiao, Y. Gu, Z. Y. Zhang, and W. G. Zhu, Nat. Commun. **8**, 14956 (2017).

[22] F. Xue, W. Hu, K.-C. Lee, L.-S. Lu, J. Zhang, H.-L. Tang, A. Han, W.-T. Hsu, S. Tu, W.-H. Chang, C.-H. Lien, J.-H. He, Z. Zhang, L.-J. Li, and X. Zhang, Adv. Funct. Mater. **28**, 1803738 (2018).

[23] J. Xiao, H. Zhu, Y. Wang, W. Feng, Y. Hu, A. Dasgupta, Y. Han, Y. Wang, D. A. Muller, and L. W. Martin, P. Hu, and X. Zhang, Phys. Rev. Lett. **120**, 227601 (2018).

[24] S. Wan, Y. Li, W. Li, X. Mao, C. Wang, C. Chen, J. Dong, A. Nie, J. Xiang, Z. Liu, W. Zhu, and H. Zeng, Adv. Funct. Mater. **29**, 1808606 (2019).

[25] C. Zheng, L. Yu, L. Zhu, J. L. Collins, D. Kim, Y. Lou, C. Xu, M. Li, Z. Wei, Y. Zhang, M. T. Edmonds, S. Li, J. Seidel, Y. Zhu, J. Z. Liu, W.-X. Tang, and M. S. Fuhrer, Sci. Adv. **4**, eaar7720 (2018).

[26] F. Zhang, Z. Wang, J. Dong, A. Nie, J. Xiang, W. Zhu, Z. Liu, and C. Tao, ACS Nano **13**, 8004 (2019).

[27] C. Cui, W.-J. Hu, X. Yan, C. Addiego, W. Gao, Y. Wang, Z. Wang, L. Li, Y. Cheng, P. Li, X. Zhang, H. N. Alshareef, T. Wu, W. Zhu, X. Pan, and L.-J. Li, Nano Lett. **18**, 1253 (2018).

[28] J. van Landuyt, G. van Tendeloo, and S. Amelinckx, Phys. Status Solidi A **30**, 299 (1975).

[29] C. Manolikas, J. Solid State Chem. **74**, 319 (1988).

[30] See Supplemental Material at http://link.aps.org/supplemental/10.1103/PhysRevLett.125.047601 for experimental details on methods and supplemental figures, which includes Refs. [21,31–39]

[31] E. J. Kirkland, *Advanced Computing in Electron Microscopy* (Springer Science & Business Media, New York, 2010).

[32] K. Osamura, Y. Murakami, and Y. Tomiie, J. Phys. Soc. Jpn. **21**, 1848 (1966).

[33] H.-G. Kim, I.-S. Min, and W.-T. Kim, Solid State Commun. **64**, 819 (1987).

[34] P. J.-C. Tedenac, D. G. P. Vassilev, B. Daouchi, J. Rachidi, and G. Brun, Cryst. Res. Technol. **32**, 605 (1997).

[35] B. H. Savitzky, I. El Baggari, A. S. Admasu, J. Kim, S. W. Cheong, R. Hovden, and L. F. Kourkoutis, Nat. Commun. **8**, 1883 (2017).

[36] R. F. Egerton, *Electron Energy-Loss Spectroscopy in the Electron Microscope* (Springer Science & Business Media, New York, 2011).

[37] Y. Shi, Y. Guo, X. Wang, A. J. Princep, D. Khalyavin, P. Manuel, Y. Michiue, A. Sato, K. Tsuda, S. Yu, M. Arai, Y. Shirako, M. Akaogi, N. Wang, K. Yamaura, and A. T. Boothroyd, Nat. Mater. **12**, 1024 (2013).

[38] A. K. Yadav, K. X. Nguyen, Z. Hong, P. García-Fernández, P. Aguado-Puente, C. T. Nelson, S. Das, B. Prasad, D. Kwon, S. Cheema, A. I. Khan, C. Hu, J. Íñiguez, J. Junquera, L.-Q. Chen, D. A. Muller, R. Ramesh, and S. Salahuddin, Nature (London) **565**, 468 (2019).

[39] S. Haussühl, *Physical Properties of Crystals* (Wiley-VCH, Weinheim, 2008).

[40] W. Feng, F. Gao, Y. Hu, M. Dai, H. Liu, L. Wang, and P. Hu, ACS Appl. Mater. Interfaces **10**, 27584 (2018).

[41] P. E. Batson, N. Dellby, and O. L. Krivanek, Nature (London) **418**, 617 (2002).

[42] C. T. Nelson, P. Gao, J. R. Jokisaari, C. Heikes, C. Adamo, A. Melville, S.-H. Baek, C. M. Folkman, B. Winchester, Y. Gu, Y. Liu, K. Zhang, E. Wang, J. Li, L.-Q. Chen, C.-B. Eom, D. G. Schlom, and X. Pan, Science **334**, 968 (2011).

[43] Y. Zhu, R. L. Withers, L. Bourgeois, C. Dwyer, and J. Etheridge, Nat. Mater. **14**, 1142 (2015).

[44] A. K. Yadav, C. T. Nelson, S. L. Hsu, Z. Hong, J. D. Clarkson, C. M. Schlepütz, A. R. Damodaran, P. Shafer, E. Arenholz, L. R. Dedon, D. Chen, A. Vishwanath, A. M. Minor, L. Q. Chen, J. F. Scott, L. W. Martin, and R. Ramesh, Nature (London) **530**, 198 (2016).

[45] R. E. Cohen, Nature (London) **358**, 136 (1992).

[46] J. Wang, J. Neaton, H. Zheng, V. Nagarajan, S. Ogale, B. Liu, D. Viehland, V. Vaithyanathan, D. Schlom, U. V. Waghmare, N. A. Spaldin, K. M. Rabe, M. Wuttig, and R. Ramesh, Science **299**, 1719 (2003).

[47] A. Schilling, T. B. Adams, R. M. Bowman, J. M. Gregg, G. Catalan, and J. F. Scott, Phys. Rev. B **74**, 024115 (2006).

[48] S. N. Shirodkar and U. V. Waghmare, Phys. Rev. Lett. **112**, 157601 (2014).

[49] S. J. Pennycook and D. E. Jesson, Phys. Rev. Lett. **64**, 938 (1990).
[50] H. L. Xin, V. Intaraprasonk, and D. A. Muller, Appl. Phys. Lett. **92**, 013125 (2008).
[51] D. Viehland, Phys. Rev. B **52**, 778 (1995).
[52] M. S. Choi, B.-K. Cheong, C. H. Ra, S. Lee, J.-H. Bae, S. Lee, G.-D. Lee, C.-W. Yang, J. Hone, and W. J. Yoo, Adv. Mater. **29**, 1703568 (2017).